IRAQI JOURNAL OF MATERIALS
Volume (5) Issue (1) January-March 2026, pp. 39-46
Published and Sponsored by American Quality for Scientific Publishing, Inc. (AQSP)

Correlation of Properties-Structures in Polycrystalline Thin Film Solar Cells Using Light-Beam-Induced Current Mapping

Sarsan T. Urhan [1], Kadhim A.K. Farhan [1,2*], Mehmet N. Kirmizgul [1]

[1] *Department of Electrical and Electronic Engineering, Faculty of Engineering, Izmir University, Izmir, TÜRKIYE*
[2] *Department of Electrical Engineering, College of Engineering, Thi Qar University, Nasiriyah, IRAQ*
** Corresponding author email: kadhim.aadim@yahoo.com*

Abstract
Light-beam-induced-current (LBIC) measurements are providing a direct link between the spatial non-uniformities inherent in thin-film polycrystalline solar cells, such as CdTe and CIGS, and the overall performance of these cells. LBIC is uniquely equipped to produce quantitative maps of local quantum efficiency with relative ease. Spatial resolution of 1 μm at 1-sun intensity, and return to the same area after other measurements, is routinely achieved. A wavelength range of 638nm to 857nm is available with diode lasers. The LBIC measurements demonstrate that several types of effects that alter cell performance can be traced to specific local-area features. Examples of such effects include defects related to edges, grids, or scribes, spatial variations in alloying, and local changes due to high-temperature stress.

Keywords: Solar cells; Polycrystalline materials; Thin films; Ligh-Beam-Induced Current technique
Received: September 2025; **Revised:** November 2025; **Accepted:** December 2025; **Published:** January 2026

1. Introduction

The composition of the gas mixture in DC reactive sputtering exerts a profound influence on the inherent structural attributes of nanostructured metal oxide thin films, directly impacting aspects such as their crystalline arrangement, elemental proportionality, particulate dimensions, outward appearance, and concentration of imperfections [1,2]. Within this sputtering process, a pure metal target is subjected to bombardment within an environment comprising both an inert gas, typically argon (Ar), and a reactive gas, such as oxygen (O_2) for oxide film formation [3]. The precise proportion of these gases directly modulates the intricate chemical reactions within the plasma, the efficiency with which material is ejected from the target, and the specific chemical interactions occurring both on the target's surface and on the developing film [4,5].

Recently, the polycrystalline thin film solar cells were considered for solar energy conversion as they showed a balance between the low fabrication cost, acceptable efficiency, and wide-range ability of production [1-3]. They were fabricated from materials such as cadmium telluride (CdTe), copper-indium-gallium sulfide (GIGS), and polycrystalline silicon (pSi) [4-6]. The performance of these materials depends on the quality of the microstructure, grain boundaries, and spatial distribution of structural and electrical defects, which strongly affect the generation mechanisms and dynamics of the charges within the solar cell and hence its optoelectronic efficiency. However, the inhomogeneous nature of these materials imposes some difficulties in describing their electrical behavior by only using the conventional bulk measurements, which may hide the precise spatial details related to the active regions or current-limiting regions [7-9]. Consequently, the need for localized diagnosis techniques with ability to correlate the microstructure to the electrical performance has increased. Such correlation allows the understanding of loss mechanisms as well as determining the locations of microstructural defects [10,11]. The light-beam-induced current (LBIC) technique is one of these techniques that provides a possibility to spatially scan the solar cell and record the electrical response due to an exact illumination spot, which enables to produce spatial maps of collection efficiency and current induced with the cell surface [12-14].

The LIBC technique depends on the illumination of consecutive points on the solar cell surface with a focused light beam while the current is measured at each point as a result of electron-hole pair production and translation to the electrodes. This mechanism provides an effective tool to study the properties of local charge collection, diffusion length, separation efficiency at the junction, and effects of

grain boundaries, and surface and internal defects [15-17]. In polycrystalline solar cells, the grain boundaries play two roles; they act as recombination centers to reduce the carrier lifetime, and sometimes they may contribute to guiding the charge motion according to their chemical and electrical structures [18,19]. Using LBIC mapping, the high-performance regions can be distinguished from degraded regions, and then related to the microstructure images or chemical compositional maps. As well, the selection of different wavelengths of the illuminating beam allow to study the deep or surface behaviors of the carriers due to the different optical absorption depths of different wavelengths. Therefore, the LIBC technique is an electrical imaging method and an integrated analytical method to understand the relationship between the microstructure and optoelectronic properties in polycrystalline thin films [20-22].

The significance of the localized analysis increases in the development strategies of thin film solar cells as a method to enhance the consecutive fabrication and treatment processes, such as thermal or chemical treatment aiming to reduce the defect density and enhance the grain boundaries [23]. Without techniques like LIBC, it is difficult to assess the actual trace of such treatments at the microscale because the overall efficiency of the cell can be enhanced whereas wide regions still suffer from invisible high loss at the intermediate measurements [24,25]. Also, the understanding of the spatial difference of electrical response contributes in developing much more accurate physical models to describe the behavior of polycrystalline solar cells and predict their performance under different operation conditions [26-28]. These studies gain special importance in the industrial applications as the control of production quality and homogenous performance over wide area represent a main challenge. By integrating the LBIC analysis with other characterization techniques, such as scanning electron microscopy or localized spectroscopic analysis, a comprehensive description can be formed to relate the structural and chemical structures to the optoelectronic performance. This would enable to enhance the design of solar cells and increase their efficiencies and long-term stabilities [29,30]. Accordingly, the study of LBIC in polycrystalline thin film solar cells is an important scientific entrance to understand and control the loss mechanisms as well as taking this technique to high levels of efficiency and reliability to achieve the goals of sustained energy programs [31-33].

Since the late 1970's, scanned laser beams have been used to measure photocurrent variations in multicrystalline silicon cells [34-36]. In the 1980's, the two-dimensional laser scanner, which used oscillating mirrors to produce a rastered response map, was developed and used to map defects in thin-film solar cells [37-39]. Improvements to the two-mirror scanner reduced the laser spot size to 2 μm [38] and introduced modern computer techniques to capture and store the data [40-43]. The two-mirror scanner, however, is not well suited to quantitative studies of small areas, since it is difficult to align and to maintain a highly focused spot over a significant area [44,45].

Instead of moving a laser beam across a solar cell, the cell can also be moved through a fixed the laser beam, either with translation stages [46] or with pieozoelectric rastering [47]. Use of a modern stepper motors makes the translation-stage approach straightforward, and one can reliably position and reposition a specific area within the beam with uncertainty much less than 1 μm [43]. It is highly desirable to be able focus the laser beam near its diffraction limit and to maintain an intensity similar to normal solar intensity. These requirements imply a laser-beam power the order of 1nW, which produces photocurrents the order of 1nA.

2. Light-Beam-Induced-Current System

The Light-Beam-Induced-Current (LBIC) configuration used to measure solar-cell response is shown in Fig. (1) [9-11]. A similar LBIC facility has been reported in Ref. [48]. In Fig. (1), the light source is selected from laser diodes of different wavelengths between 638nm and 850nm. Current to the laser diode is electronically modulated to produce an AC laser beam, and the modulation also provides the reference signal for a lock-in amplifier. Attenuation over a wide dynamic range is set with digital control. The beam is expanded, the s-polarization is selected, and the beam is sampled for both intensity and back-reflection from the cell. Beam steering mirrors allow a parallel beam to impinge on the objective lens (Olympus 1-UB367 SLC Plan Fluoride 40x/0.55 N.A.). This lens is equipped with a correction collar to focus through 0-2.5 mm of glass. It has a working distance of 8.8mm, which allows ample room for contacts.

LBIC measurements using the apparatus shown in Fig. (1) are made by stepping the solar cell under study through the focused beam in a raster pattern. The stepping distance is generally set to half the beam size. Data collection takes approximately 20 min to produce a photocurrent map of 101 by 101 points for a small area, and somewhat longer for larger areas requiring greater travel distances.

IRAQI JOURNAL OF MATERIALS
Volume (5) Issue (1) January-March 2026, pp. 39-46
Published and Sponsored by American Quality for Scientific Publishing, Inc. (AQSP)

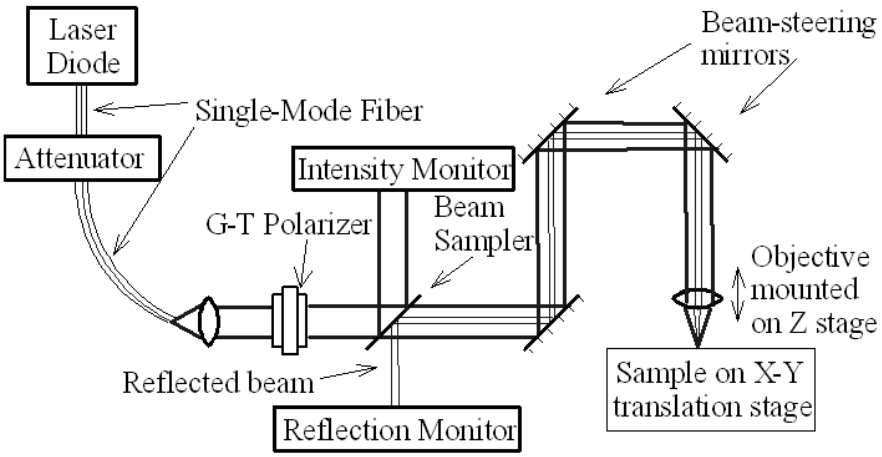

Fig. (1) Schematic of Light-Beam-Induced-Current LBIC apparatus

3. Data Presentation

Our LBIC data is commonly presented in one of three formats as illustrated in Fig. (2). The top figure shows an intensity projection of a CIGS solar cell with the grid fingers clearly visible. The middle figure for the same cell is the most common format, the local-area quantum-efficiency (QE) map of the area of interest. This format clearly illustrates an isolated feature with low response. The bottom format repeats the same CIGS data in a histogram format, which more clearly emphasizes the spread in QE over the cell.

Three standard resolutions are used, and these are illustrated in Fig. (3) for an NREL-manufactured CIGS cell. Low resolution, shown at the top, has a 5mm field and a 100μm spot. This resolution often covers a significant portion of a typical test cell. The small square in this view is magnified ten times for the middle map at mid resolution (500 by 500μm field and 10μm spot). The area shown in that map's small square in multiplied 10 times more for the 50 by 50μm field with a 1μm spot for the high resolution map at the bottom of Fig. (3).

In each case the beam was attenuated so that intensity at the cell was comparable to one sun. This process makes it straightforward to zoom in on a small area of particular interest and to return to the same area even after the cell has been removed from the apparatus for other measurements. The bottom high-resolution map, for example, shows several features that are 2-5 microns in dimension that are only marginally seen at lower resolution.

The quantum-efficiency maps shown in Fig. (3) all have a scale to show QE changes of 2%. This scale is varied as needed to match the total variation of interest. For example, 1% gradations were used in the middle section of Fig. (2). In general, the average QE of the LBIC maps agrees quite well with QE measured with a conventional system. All of the data shown in Figs. (2) and (3) were taken at zero bias and a wavelength of 638 nm, which will be taken as standard unless otherwise stated.

The most common LBIC features are local optical blockages that reduce the photocurrent over small, well-defined areas. Their characteristic signature is sharp edge definition, and they can result from inclusions during fabrication. They are most likely what is seen in the middle section of Fig. (2) and the bottom section of Fig. (3). In some cases, there is an accompanying increase in reflection that gives a nearly identical map over the same area. There are two other possibilities, however, which have a similar signature to an optical impediment. One is a local area that does not collect photocarriers efficiently, and the other is a region where adjacent layers have not made good electrical contact. The latter situation often extends over larger regions than the features seen in Figs. (2) and (3).

A third category of LBIC features is what we term external. These features can result, for example, from blemishes in a flexible substrate, from the pressure applied by measurement probes, or simply from dust particles on the surface. One consequence of the large number of possibilities for LBIC features is that it is rare to find a cell, even the best space-qualified cell, where the LBIC map is completely uniform.

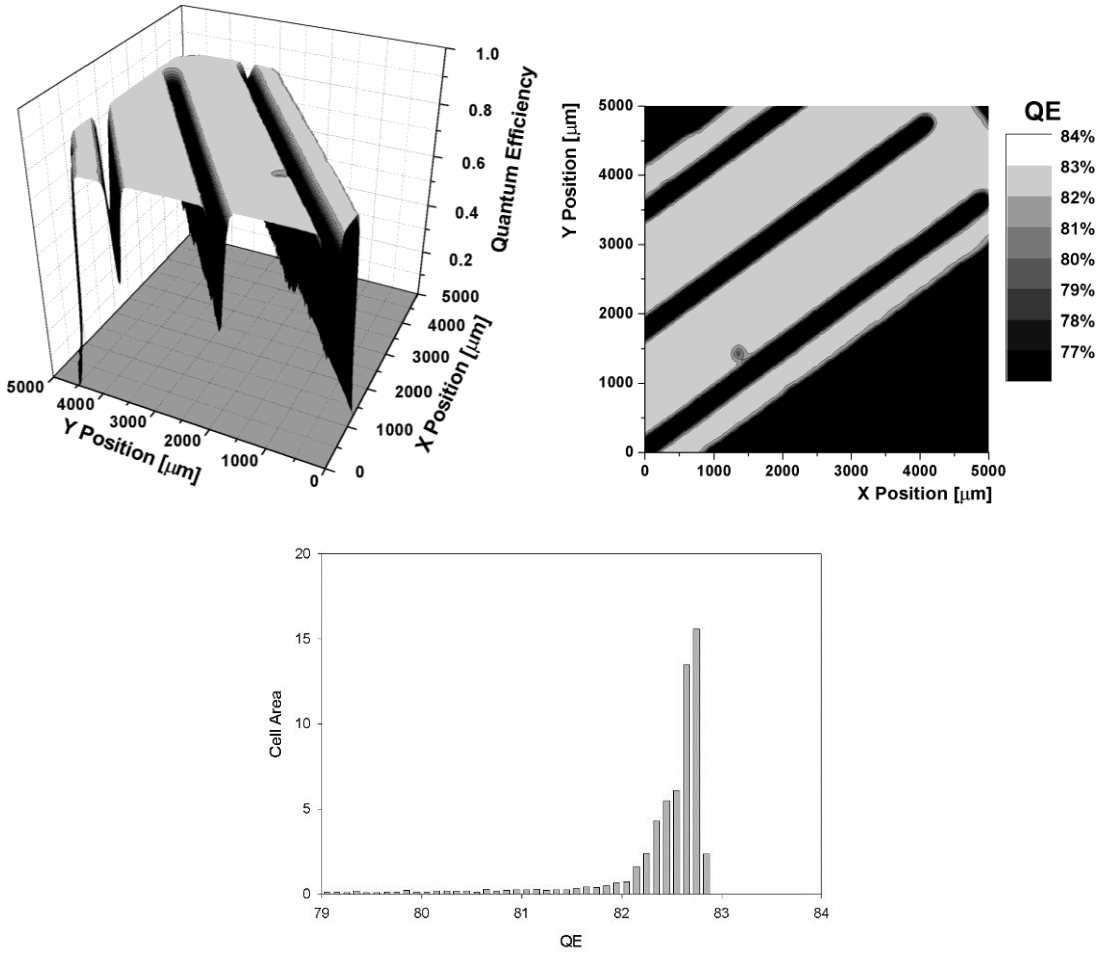

Fig. (2) Three LBIC formats (low resolution)

The second major category of LBIC features is a leakage path, which could be either a filamentary shunt or a weak diode. The latter tends to be very bias dependent. In either case, the actual flaw can be very small, but the photocurrent reduction will spread over a much larger area.

LBIC measurements are particularly valuable to help explain changes sometimes seen in CdTe solar cells that have been subjected to elevated-temperature stress. The general observation is that when the performance of a cell changes during such stress, the changes are essentially never uniform over the entire cell. The result is an increase in the non-uniformity seen in LBIC measurements. An example is given in Fig. (5), which shows a low-resolution, whole-cell map before any stress, after 8 hours, and after 8 days at a temperature of 100ºC under illumination and short-circuit conditions. The average QE decreased by about 2% over 8 days, which is reflected in the current-voltage (J-V) curve, but there were small areas where the reduction was significantly larger.

In many cases, the impact of elevated-temperature stress on both J-V and LBIC data varies significantly with differences in cell fabrication. One example reported earlier [49,50] was much larger non-uniformities generated in CdTe cells made with insufficient copper in the back contact. Another example, illustrated in histogram format in Fig. (4), contrasts two CdTe cells that differed in another aspect of fabrication. Both cells had very uniform QE initially. After exposure to 30 days of elevated-temperature stress, the cell in the top panel with standard back-contact processing showed only a modest decrease in average QE and uniformity. However, the cell depicted in the bottom QE histogram, which was made with part of the contact procedure omitted, showed much larger reductions in both the magnitude and uniformity of its QE.

ISSN (print) 2958-8960 (online) 3006-6042

IRAQI JOURNAL OF MATERIALS
Volume (5) Issue (1) January-March 2026, pp. 39-46
Published and Sponsored by American Quality for Scientific Publishing, Inc. (AQSP)

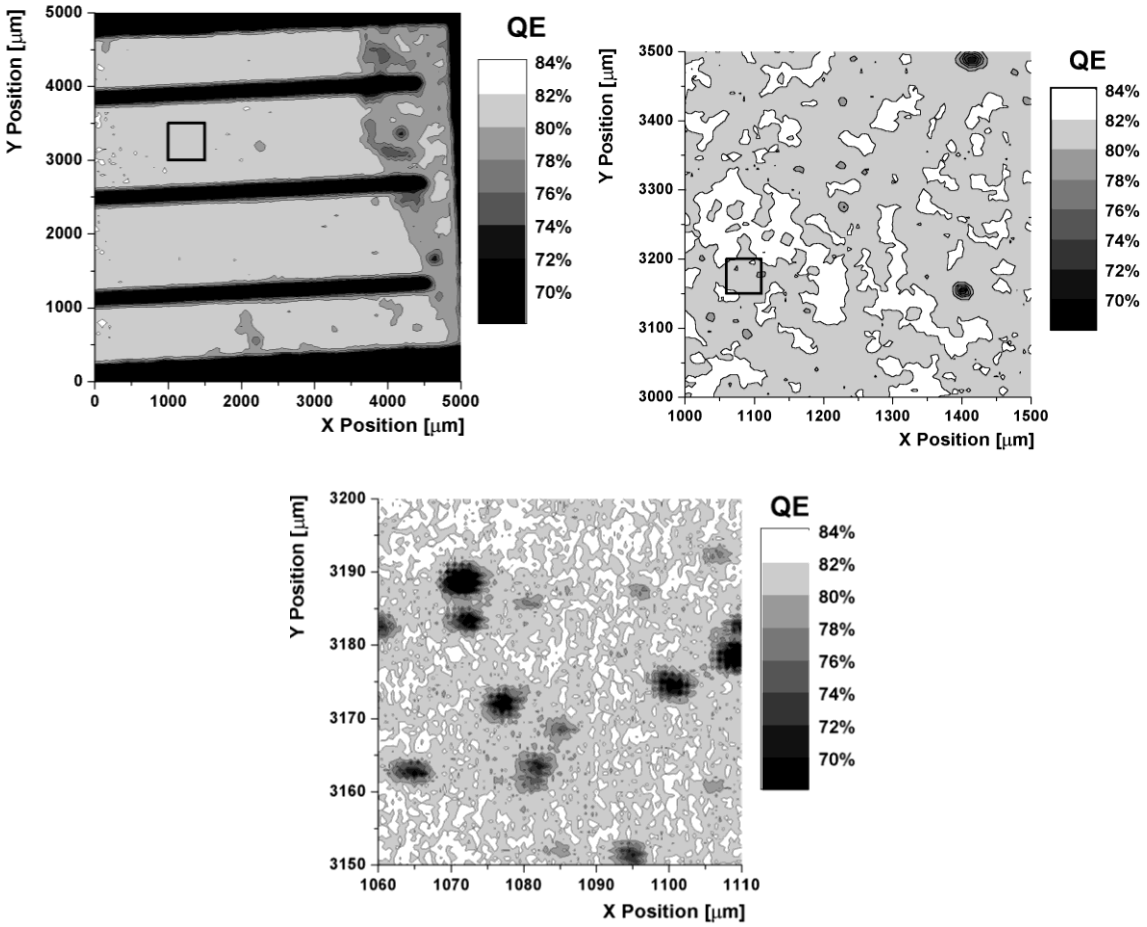

Fig. (3) LBIC with low-, mid-, and high-resolution (100-, 10-, and 1-micron spots)

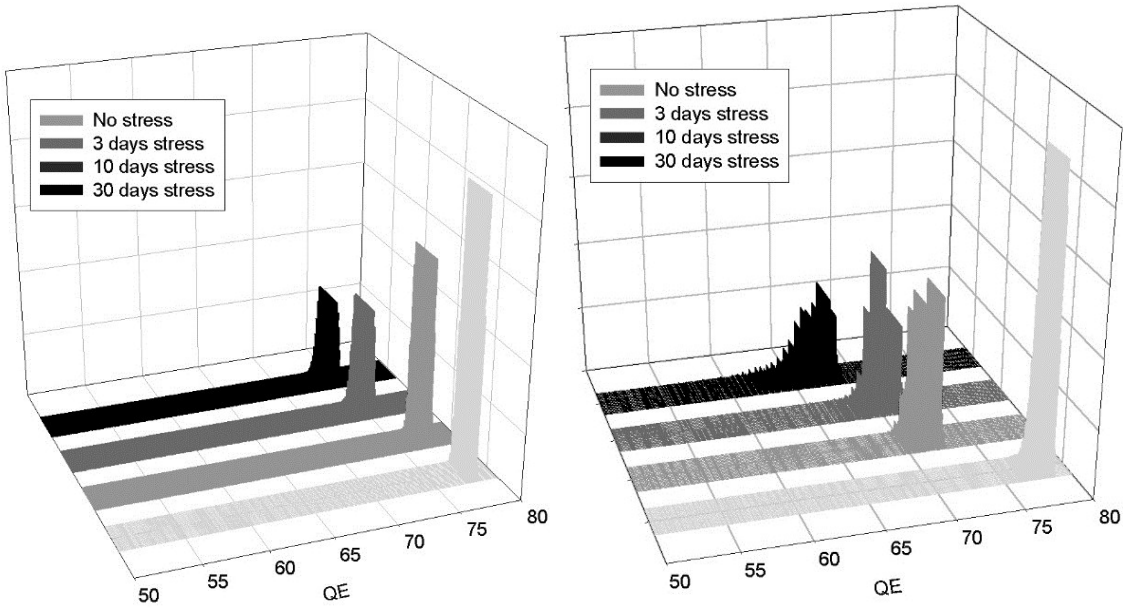

Fig. (4) Contrasting effect of stress on two CdTe cells made with and without a key contacting step

4. Wavelength and Bias Variations

The ability to vary the wavelength used for LBIC measurements is particularly valuable if wavelength can be scanned through the absorber band gap. One of our laser diodes was chosen so that its wavelength could be varied from 830 to 860nm, which spans the CdTe band gap, by varying its temperature. An earlier report [10] showed that this technique could be used with high-resolution LBIC to observe the band-gap variations due to spatial variations in CdTe/CdS mixing.

Variations of LBIC maps as a function of cell bias has also proven useful. In this case, improvements in the detection electronics were required to adequately separate the ac LBIC signal from the dark dc response of the cell. With care, LBIC data can now be taken at bias up to the cell's open-circuit voltage.

An example of LBIC bias dependence is shown in Fig. (5). The top figure shows the J-V curve from two CIGS cells made with different concentrations of gallium.

The cell with the better-behaved J-V curve had a uniform LBIC response at all biases. The magnitude of the LBIC signal, however, did decrease when the J-V curve turned up following the expected behavior of the apparent quantum efficiency [51,52]. The mid-resolution LBIC response from the "distorted" J-V curve (Fig. 5), however, showed a decrease in average magnitude at relatively low bias. Furthermore, even at the relatively low 200mV bias, LBIC shows significant non-uniformity.

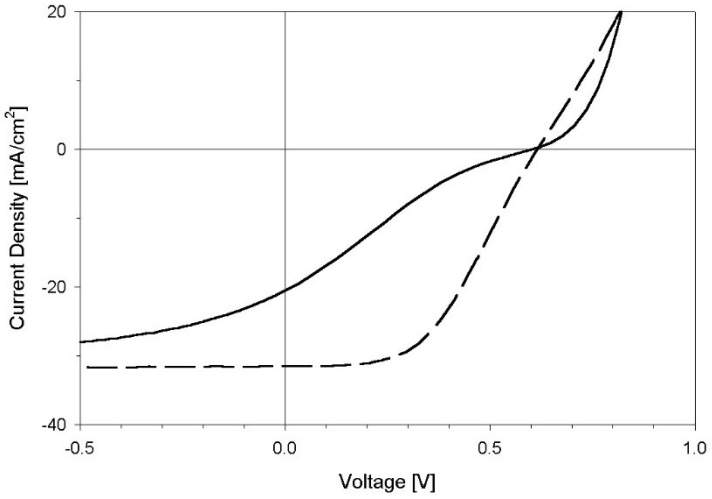

Fig. (5) J-V curve of a reasonably well-behaved CIGS cell (dashed) and a highly distorted one (solid)

5. Conclusions

LBIC has become a reliable tool for investigating a variety of solar-cell non-uniformities. It has become much more practical in recent years with improvements in translation stages, laser diodes, and data-handling techniques. LBIC is particularly valuable to help explain differences due to processing variations or changes induced by elevated-temperature stress. It can be reliably combined with other small-area investigation techniques to study the same area at different labs. Finally, in our experience, poorer performing cells almost always show larger LBIC variations indicative of poorer uniformity.

References

[1] B. Bhushan (Ed.), **"Springer Handbook of Nanotechnology"**, Springer, p. 27, 151, 438 (2004).
[2] M.C. Gupta and J. Ballato (editors), **"The Handbook of Photonics"**, 2nd ed., CRC Press, Taylor & Francis Group (FL), Ch. 8, 1-27 (2007).
[3] P.M. Martin, **"Handbook of Thin Film Deposition Techniques"**, Elsevier, p. 4 (2010).
[4] M. Ladd and R. Palmer, **"Structure Determination by X-Ray Crystallography"**, 5th ed., Springer (NY), p. 568 (2013).
[5] S.K. Kulkarni, **"Nanotechnology: Principles and Practices"**, 3rd ed., Springer (Cham), p. 295 (2015).
[6] M. Grundmann, **"The Physics of Semiconductors"**, 3rd ed., Springer (Cham), 461-487 (2016)
[7] S.F. Bertram, **"Handbook of X-rays"**, ed. E.F. Kaelbe, McGraw-Hill (NY), p. 817 (1976).
[8] H.-L. Chen, Y.-M. Lu and W.-S. Hwang, "Effect of Film Thickness on Structural and Electrical Properties of Sputter-Deposited Nickel Oxide Films", Mater. Trans., 46(4), 872-879 (2005).
[9] J. Cui, S. Chen, H. Liu and Z. Huang, "Nano-p–n junction heterostructures enhanced TiO_2 nanobeltsbiosensingelectrode", J. Solid State Electrochem., 18, 2693-2699 (2014).
[10] K.O. Ukoba and F.L. Inambao, "Modeling of Fabricated NiO/TiO_2 P-N Heterojunction Solar Cells", Int. J. Appl. Eng. Res., 13(11), 9701-9705 (2018).

[11] A.H. Aka et al., "Synthesis and characterization of kesterite $Cu_2ZnSn(S_xSe_{1-x})_4$ thin films with low-cost for efficient solar cells", Result Opt., 13 (2023) 100507.
[12] A.J. Olivares et al., "Boron activation in silicon thin films grown by PECVD under epitaxial and microcrystalline conditions", Appl. Surf. Sci. Adv., 18 (2023) 100508.
[13] K.O. Ukoba and F.L. Inambao, "Study of Optoelectronic Properties of Nanostructured TiO_2/NiO Heterojunction Solar Cells", Proc. World Cong. on Eng. Comp. Sci. 2018, Vol I (WCECS 2018), October 23-25, 2018, San Francisco, USA.
[14] N.K. Das et al., "Effect of substrate temperature on the properties of RF sputtered CdS thin films for solar cell applications", Result Phys., 17 (2020) 103132.
[15] S.H. Faisal and M.A. Hameed, "Heterojunction Solar Cell Based on Highly-Pure Nanopowders Prepared by DC Reactive Magnetron Sputtering", Iraqi J. Appl. Phys., 16(3) (2020) 27-32.
[16] K.O. Ukoba, F.L. Inambao and A.C. Eloka-Eboka, "Fabrication of Affordable and Sustainable Solar Cells Using NiO/TiO_2 P-N Heterojunction", Int. J. Photoenergy, Vol. 2018, Article ID 6062390, DOI: 10.1155/2018/6062390
[17] L.C. Sim, K.W. Ng, S. Ibrahim and P. Saravanan, "Preparation of Improved p-n Junction NiO/TiO_2 Nanotubes for Solar-Energy-Driven Light Photocatalysis", Int. J. Photoenergy, Vol. 2013, Article ID 659013, DOI: 10.1155/2013/659013
[18] O. Oklobia et al., "Development of arsenic doped Cd(Se,Te) absorbers by MOCVD for thin film solar cells", Sol. Ener. Mater. Solar Cells, 231 (2021) 111325.
[19] A.K. Sen Gupta et al., "Characterizations of extrinsically doped CZTS thin films for solar cell absorbers fabricated by sol-gel spin coating method", Appl. Surf. Sci. Adv., 13 (2023) 100352.
[20] A.K. Mahmud Hasan et al., "Optoelectronic properties of electron beam-deposited NiO_x thin films for solar cell application", Result Phys., 17 (2020) 103122.
[21] H. Trivedi et al., "Investigating optical, structural and morphological properties of polycrystalline CdTe thin-film deposited by RF magnetron sputtering", Mater. Lett.: X, 11 (2021) 100087.
[22] M.A. Behnajady, N. Modirshahla, M. Shokri, H. Elham and A. Zeininezhad, "The effect of particle size and crystal structure of titanium dioxide nanoparticles on the photocatalytic properties", J. Environ. Sci. Health Part A, 43, 460-467 (2008).
[23] O.A. Hamadi, B.A.M. Bader and A.K. Yousif, "Electrical Characteristics of Silicon p-n Junction Solar Cells Produced by Plasma-Assisted Matrix Etching Technique", Eng. Technol. J., 26(8) (2008) 995-1001.
[24] Y. He et al., "Downshifting and antireflective thin films for solar module power enhancement", Mater. Design, 201 (2021) 109454.
[25] T.-Y. Lin et al., "Alkali-induced grain boundary reconstruction on Cu(In,Ga)Se_2 thin film solar cells using cesium fluoride post deposition treatment", Nano Energy, 68 (2020) 104299.
[26] V.A. Owoeye et al., "Effect of precursor concentration on stoichiometry and optical properties of spray pyrolyzed nanostructured NiO thin films", Heliyon, 9(1) (2023) e13023.
[27] N.V. Loi et al., "Enhancing the absorption figure of merit on solution-based CuO thin films by Ni doping", Opt. Mater.: X, 19 (2023) 100246.
[28] N. Xiao et al., "Current research on the design, properties and applications of tribological materials: a review", RSC Adv., 15(41) (2025) 34669-34717.
[29] M. Matsuzaka et al., "Observation of magnetoresistance effect in $Ni_{78}Fe_{22}$/tris-(8-hydroxyquinoline) erbium (Erq_3)/FeCo organic spin valves", J. Magn. Magn. Mater., 630 (2025) 173465.
[30] M.M. Shahidi et al., "Green synthesis of Cu_2S using garlic-derived sulfur: structural, morphological, optical, electrical, and photoresponse characterization with potential for thermoelectric applications", RSC Adv., 15(5) (2025) 3406-3415.
[31] Z. Wang et al., "Advanced flexible organic near-infrared photodetectors for sensing applications", Wearable Electron., 2 (2025) 124-148.
[32] C.M. Costa et al., "An overview of solid-state lithium metal batteries: Materials, properties and challenges", EnergyChem, 7(5) (2025) 100169.
[33] M.A. Dias, R. Dohmen, and N. Hartmann, "Diffusion of Eu, Ce and Lu in orthopyroxene", Geochimica et Cosmochimica Acta, 410 (2025) 85-100.
[34] M. Dorri, M.R. Anil Kumar, and K. Zaghib, "In operando and in situ characterization tools for advanced rechargeable batteries: Effects of electrode origin and electrolyte", J. Power Sour., 658 (2025) 238188.
[35] J.H. Liang et al., "Adhesion-induced MoS_2 layer transfer via in-situ TEM-nanoindentation: Effects of curvature and substrate mediated residual stress", Appl. Surf. Sci. Adv., 25 (2025) 100686.
[36] W. Sohn et al., "Advances in resistive switching memory: comprehensive insights into ECM mechanisms through TEM observations and analysis", Mater. Adv., 6(13) (2025) 4158-4173.
[37] M.I. Hossain et al., "The prospective contribution of kesterites to next-generation technologies", Nano-Struct. Nano-Objects, 42 (2025) 101480.
[38] G.A.Q. Abdulrahman et al., "2D Materials: Synthesis, properties, and energy-related applications", Coord. Chem. Rev., 544 (2025) 216950.
[39] J.H. Zhuang et al., "Recent progress in two-dimensional materials: From emerging structures and synthesis approaches to electronic and sensing applications", Chem. Eng. J., 520 (2025) 166133.
[40] K. Neuhaus, P. Mowe, and M. Winter, "Promoting combined AFM-electrochemistry techniques for analysis of charge transport at grain boundaries of ceramic components in electrochemical cells", RSC Appl. Interfaces, 2(3) (2025) 620-633.
[41] J. Yu et al., "Recent advances and future prospects of Space Materials Science", Rev. Mater. Res., 1(2) (2025) 100065.
[42] A.A. Faremi et al., "SCAPS 3201 simulation of tunable heterostructured p-CdTe and n-CdS thin films-based solar cells", Result Eng., 18 (2023) 0101039.
[43] A. Joy et al., "Numerical studies on a ternary $AgInTe_2$ chalcopyrite thin film solar cell", Heliyon, 9(8) (2023) e19011.
[44] S. Lamichhane et al., "Studies on photovoltaic properties of BFO/WO_3 bilayer thin films for solar energy harvesting applications", Result Opt., 13 (2023) 100539.
[45] G.R. Neupane et al., "Imaging local luminescence variations in $CdSe_{0.1}Te_{0.9}$ thin films grown by the colossal grain growth process", Cell Rep. Phys. Sci., 4(8) (2023) 101522.
[46] K. Monga et al., "Fabrication and characterization of Al/Ta thin films as metal junctions for solar cell applications", Mater. Lett.: X, 17 (2023) 100174.
[47] C.-C. Tseng et al., "Cu_2O-HTM/SiO_2-ETM assisted for synthesis engineering improving efficiency and stability with

heterojunction planar perovskite thin-film solar cells", Sol. Ener., 204 (2020) 270-279.
[48] Y. Tang et al., "Dynamic beam shaping with polarization control at the image plane for material processing", Procedia CIRP, 74 (2018) 581-584.
[49] E.C. Nwanna, P.E. Imoisili, and T.-C. Jen, "Synthesis and characterization of SnO_2 thin films using metalorganic precursors", J. King Saud Univ. – Sci., 34(5) (2022) 102123.
[50] Md.M. Alam Moon et al., "Unveiling the prospect of a novel chemical route for synthesizing solution-processed CdS/CdTe thin-film solar cells, Energy Rep., 7 (2021) 1742-1756.
[51] A.A. Faremi et al., "Engineering of window layer cadmium sulphide and zinc sulphide thin films for solar cell applications", Result Eng., 16 (2022) 100622.
[52] G. Liang et al., "Ion doping simultaneously increased the carrier density and modified the conduction type of Sb_2Se_3 thin films towards quasi-homojunction solar cell", J. Materiomics, 7(6) (2021) 1324-1334.

 ISSN (print) 2958-8960 (online) 3006-6042 Printed in IRAQ